International Journal of Aeronautical and Space Sciences (2022) 23:1033–1042
https://doi.org/10.1007/s42405-022-00492-1

IJASS International Journal of Aeronautical and Space Sciences

ORIGINAL PAPER

Integrated Optimization Design Using Improved Pigeon-inspired Algorithm for a Hypersonic Vehicle Model

Zaigui Wu[1] · **Yanbin Liu**[2]

Received: 13 December 2021 / Revised: 13 April 2022 / Accepted: 23 May 2022 / Published online: 22 July 2022

Abstract
Hypersonic vehicles are significantly valuable for military and civilian application due to distinctive flight features. However, hypersonic vehicles integrate multidisciplinary technologies that lead to the complicated interaction. As a result, the optimization design is critical for hypersonic vehicles to achieve the satisfactory flight performance. This paper studies the optimization strategies based on the improved pigeon-inspired optimization algorithm (PIO) for hypersonic vehicles. First, an improved algorithm is presented by introducing the Gaussian mutation into the basic PIO algorithm to maintain the swarm diversity and to avoid premature convergence. Then, the optimized issues related with the flight control system are considered, and the improved PIO algorithm is applied to search the optimized cruise state, to adjust the anticipated control parameters, and to obtain the satisfactory climbing trajectory for hypersonic vehicles. After that, the track controller is designed to ensure the system stability and to follow the optimized trajectory. Finally, a simulation example is provided to verify the effectiveness of the proposed methods for hypersonic vehicles.

Keywords Hypersonic vehicles · Integrated design · Improved Pigeon-inspired optimization algorithm · Flight control · Trajectory optimization

1 Introduction

Hypersonic vehicles (HSVs) have become a hotspot technology in international military research for their remote rapid strike and strong penetration capabilities [1], which are of considerable military and civilian value [2]. At present, studies mainly focus on the structural and control system designs of HSVs. In preliminary design, multidisciplinary optimization under different constraints and mission demands is a key component of mission deployment for HSVs [3]. In particular, the integrated methods of the elevon sizes and the center of the gravity introduce the control action to the conceptual design for hypersonic vehicles [4], and the compromise performances can be met with the multidisciplinary demands, thereby decreasing the design cost and realizing the integrated iteration [5].

The multidisciplinary optimization design of hypersonic vehicles depends on the feasible optimization strategies and algorithms. In addition, the optimization process needs to consider the numerous design variables and constraints concerning aerodynamics, structure, engine, and control [6]. Therefore, the development of the novel strategies and algorithms are very important for hypersonic vehicles to rapidly obtain the effective results and to significantly improve the design efficiency [7]. Currently, the optimization design consists of indirect and direct methods. Among them, the indirect method relies on the gradient information and acquires the optimal results using the analytic mean, whereas the direct method directly transforms the optimization problem into a parameter optimization problem without gradient information and obtains the optimal results using the numerical method [8]. Compared with the indirect method, the direct method is more suitable to solve the multidisciplinary optimization design problem of hypersonic vehicles, because this is a very complex optimization problem involving a lot of variables and constraints, and the gradient information tends to be difficult to identify [9]. Specifically, a conceptual pro-

B Yanbin Liu
liuyb@nuaa.edu.cn

1 The Research Institute of Pilotless Aircraft, Nanjing University of Aeronautics and Astronautics, Nanjing 210016, China

2 College of Astronautics, Nanjing University of Aeronautics and Astronautics, Nanjing 210016, China

totypical multifidelity, multistrategy, and multidisciplinary design optimization environment (M3 DOE) was development in [10] for complex air–vehicle configurations to obtain an optimum design with desired accuracy within the allowable design development time constraint. Alternatively, a optimization method was proposed in [11] using the genetic algorithm for optimization of hypersonic air-breathing aircraft design, which allows a wide range of designs to be evaluated ranging from wingbody configurations to all-body configurations.

Beyond this, the design of the reference trajectory for an HSV is a challenging task due to the vehicle's high nonlinearity and multiple constraints [12]. Given the difficulty of achieving the analytical solution of the trajectory optimization problem, numerical methods are involved in trajectory design, among which the direct trajectory optimization technique is the most popular [13]. The direct method avoids the premature convergence problem and is insensitive to initial conditions [14]. In addition, the direct optimization uses the pseudospectral method to merge with indirect optimization, thereby improving its computational efficiency [15]. In particular, the Gaussian pseudospectral method was applied in [16] to transcribe the optimal control problem into a nonlinear programming problem by approximating the state and control at a set of discrete points. Similarly, second-order cone programming was utilized in [17] to the class of highly nonlinear trajectory optimization problems in entry flight, and a nonlinear estimation algorithm polynomial chaos theory was proposed in [18] to estimate state trajectories of a hypersonic vehicle with initial condition uncertainty and to predict the evolution of state uncertainty of the nonlinear system. Not only that, a new multi-objective method to the aircraft climb path optimization problem was presented in [19] using the particle swarm optimization algorithm. Furthermore, an artificial bee colony (ABC)-based direct collocation method was proposed in [20] for reentry trajectory optimization, and the control variables were discretized at a set of Legendre–Gauss collocation points and were optimized with the ABC approach. These studies indicate that the intelligent optimization method is an effective tool to solve the complex optimization problem, and this stimulates us to develop an intelligent optimization algorithm for hypersonic vehicles.

The pigeon-inspired optimization (PIO) algorithm can identify rapidly the results for the complex multidisciplinary design problem, and is suitable for the application to the hypersonic vehicle. However, the original PIO algorithm is easy to fall into local optimization due to lack of the diversity of the population; thus, this algorithm needs to be improved to meet the requirements of convergence accuracy and iteration efficiency for HSVs. To this end, this paper proposes an improved pigeon-inspired optimization (PIO) algorithm to address the optimization problem of HSVs. This work aims to utilize an improved intelligence optimizer to tackle the optimization problem while avoiding computational difficulty. The main contents of this paper include (1) the improvement of the basic PIO algorithm with first Gaussian mutation to improve the algorithm's swarm diversity for search space exploration and modification of the fitness function with penalty function to deal with the equality and inequality constraints of the typical trajectory optimization problem, (2) the application of the improved PIO algorithm in determining the optimal cruise state for a succeeding climbing trajectory, and (3) the utilization of the improved PIO algorithm to the climbing trajectory optimization problem. Finally, a simulation example is given to validate the effectiveness of the proposed optimization methods for HSVs.

2 Improved Pigeon-Inspired Optimization Algorithm

The basic PIO algorithm is a new swarm intelligence method that is inspired by natural pigeons' outstanding homing behavior. Investigations of pigeons' homing abilities show that they mainly rely on small magnetic particles in their beaks during navigation [21]. These iron crystals provide north-pointing capability, and signals are transmitted to their brains via trigeminal nerves. Studies reveal that the sun is involved in pigeons' navigation system and that they can distinguish the sun's altitude between a start point and their current location to help determine their course [22]. Recent studies find that pigeons can follow certain landmarks during their course rather than head for their destinations directly [23]. By simulating pigeons' natural mechanism, the PIO algorithm can increase feasibility for complicated optimization problems [24].

The PIO algorithm consists of two individual operators, including the map and compass operator and the landmark operator. In the algorithm, the population size and dimension of the problem are described by N and n, respectively. Each pigeon in the flock represents a possible solution and corresponds to a fitness value [21]. The pigeon k is associated with a position vector $X(k)$ and a velocity vector $V(k)$ in the form of

$$X(k) = [x_1(k), x_2(k), \ldots, x_n(k)], \quad (k = 1, 2, \ldots, N), \tag{1}$$

$$V(k) = [v_1(k), v_2(k), \ldots, v_n(k)], \quad (k = 1, 2, \ldots, N). \tag{2}$$

In the map and compass operator, all pigeons update their position according to the best position in the flock. Accordingly, the velocity and position vectors are updated as

$$V^{(t)}(k) = V^{(t-1)}(k) \cdot \mathrm{e}^{-Rt} + \mathrm{rand} \cdot \left(g_{\mathrm{best}}^{(t-1)} - X^{(t-1)}(k)\right), \tag{3}$$

$$X^{(t)}(k) = X^{(t-1)}(k) + V^{(t)}(k), \tag{4}$$

where t is the current iteration, R is the map and compass factor, $g_{\text{best}}^{(t-1)}$ is the best position in the flock, and rand is a random number between 0 and 1.

In the landmark operator, half of the pigeons follow those who are close to landmarks, and the center of these chosen pigeons can be obtained by

$$C^{(t)} = \frac{\sum_{N_\text{P}} X^{(t)}(k) \cdot \text{fitness}\left(X^{(t)}(k)\right)}{\sum \text{fitness}\left(X^{(t)}(k)\right)}, \tag{5}$$

where fitness() is the objective function of the problem and N_P is the number of pigeons in the current iteration, which is halved in each iteration.

As in most classical intelligent algorithms, the individuals of the swarm in PIO tend to converge during iteration, which may result in premature convergence in the handling of complicated multimodal problems. To increase the space exploration capability of the algorithm, the diversity is introduced in the PIO algorithm.

(1) Quantification of diversity

The diversity identifies the difference between individuals in the population, and such difference is quantified by the Euclidean distance. There are three forms of quantification of diversity: the design variable diversity $D_{v,t}$, individual diversity $D_{p,t}$, and diversity of the swarm $D_{s,t}$. Furthermore, the diversity can be defined by the global position of individuals which can be described as three following ways: the difference between individuals and the best individuals, the difference between individuals and the average individuals, and the difference between all individuals. Among them, individual diversity is computed by

$$D_{p,t}\big|_{t=1,2,\ldots,T}^{p=1,2,\ldots,s} = \left[\sum_{j=1}^{d} (x_{i,j}(t) - \bar{x}_j(t))^2\right]^{\frac{1}{2}}, \tag{6}$$

$$\bar{x}_j(t) = \frac{1}{s}\sum_{i=1}^{s} x_{i,j}(t). \tag{7}$$

Also, the diversity of the swarm is calculated by

$$D_{s,t} = \frac{1}{s}\sum_{i=1}^{s}\left[\sum_{j=1}^{d} (x_{i,j}(t) - \bar{x}_j(t))^2\right]^{\frac{1}{2}}. \tag{8}$$

The diversity of the swarm is usually used in intelligent optimization algorithms to reflect the diversity of the population and the local searching ability.

(2) Gaussian mutation-based PIO algorithm

The Gaussian mutation-based PIO algorithm (GPIO) is an improved method that uses a Gaussian mutation operator to enhance the diversity of the basic PIO algorithm and thus to improve the space exploration capability [25]. The mutation operator promotes diversity by changing a pigeon's dimension value using a random number drawn from the Gaussian distribution.

In this algorithm, the mutation operator is activated only when the diversity of the swarm becomes less than a certain threshold d_{low}. The velocity vector is updated as Eq. (1), and the position vector is updated based on the following criteria:

$$x_{i,j}(t) = x_{i,j}(t-1) + \xi R_a, \tag{9}$$

where ξ is the weight number and R_a is a random number that follows the Gaussian distribution.

Penalty functions are commonly used to solve constrained optimization problems. With the construction of a penalty term, the constrained optimization problem is converted into an unconstrained optimization problem. In this research, the penalty function is built as

$$\bar{P}(x) = \sum_{i=1}^{l} H_i^2(x) + \sum_{i=1}^{m} [\min\{0, G_i(x)\}]^2, \tag{10}$$

where H and G represent equality constraints and inequality constraints, respectively. Accordingly, the constraints in the optimization are transformed into the penalty value in the performance index, and the required optimal solution can be obtained by solving this unconstrained optimization problem. The augmented fitness function with penalty function is described as

$$fitness(x) = J_{\min} = J_0 + \sigma \bar{P}(x), \tag{11}$$

where σ is the penalty term and J_0 is the original fitness function.

3 Nonlinear Model and Dynamics Characteristics of Hypersonic Vehicles

Hypersonic vehicles have brought tremendous challenges to the overall and control system design due to the high Mach number and wide flight range. Currently, the typical configuration of hypersonic vehicles mainly includes the conical body, lifting body, waverider, and so on, and this study adopts the waveriding configuration [26], and the geometric shape is depicted in Fig. 1.

After constructing the geometric shape of the waverider, the surface element and engineering estimation methods are

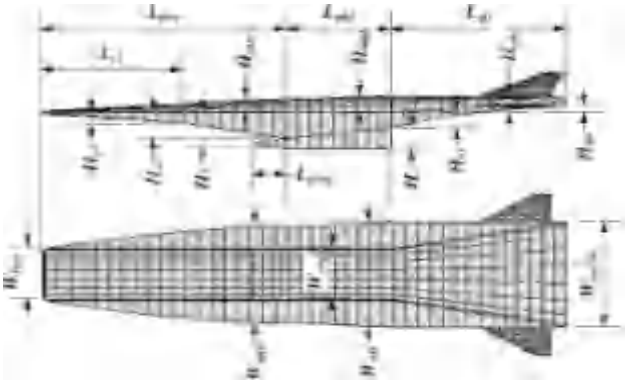

Fig. 1 The geometric configuration of hypersonic vehicles

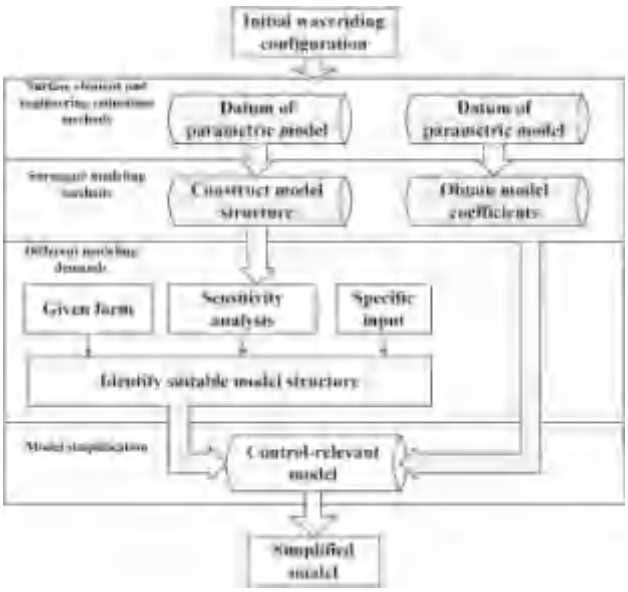

Fig. 2 The design flowchart of the control-oriented model

used to obtain the model parameters [27], and furthermore, the control-relevant model is derived based on these acquired parameters using the surrogate modeling method [28]. The design flowchart of the control-oriented model is shown in Fig. 2.

The acquisition of the control-relevant model consists of four steps: selecting the sample points, identifying the model structure, obtaining the model coefficients, and validating the simplified model. First, the sample points are selected based on the Latin hypercube sampling method with higher sampling efficiency and less operation time. After that, the model structure is identified on the basis of the results of sensitivity analysis regarding each model variable. Furthermore, the model coefficients are obtained using the system identification method, and the final step is to verify the effectiveness of the control-oriented model. Furthermore, the specific expressions of the force and moment coefficients are identified as

$$\begin{cases} C_L = \frac{C_L^0+C_L^\alpha\alpha+C_L^\delta\delta_e}{\sqrt{Ma^2-1}} \\ C_D = C_D^0 + C_D^\alpha\alpha+C_D^\delta\delta_e+C_D^{\alpha\delta}\alpha\delta_e \\ \quad +C_D^{\alpha^2}\alpha^2+C_D^{\delta^2}\delta_e^2+C_D^{Ma}\frac{1}{Ma^2} \\ C_m = C_m^0 + C_m^\alpha\alpha + C_m^\delta\delta_e + C_m^{\alpha\delta}\alpha\delta_e \\ \quad +C_m^{\alpha^2}\alpha^2 + C_m^{\delta^2}\delta_e^2+C_m^{Ma}Ma \\ C_T = C_T^0 + \phi\left(C_{T,\phi}^\alpha\alpha + C_{T,\phi}^{\alpha Ma}\frac{\alpha}{Ma} + C_{T,\phi}^{Ma}\frac{1}{Ma}\right) \\ \quad +C_T^\alpha\alpha + C_T^{\alpha Ma}\frac{\alpha}{Ma} + C_T^{Ma}\frac{1}{Ma}, \end{cases} \tag{12}$$

where phi indicates the fuel equivalence ratio; $C_L^0, C_L^\alpha, C_L^\delta$ are the adjusted parameters concerning the lift coefficient C_L; $C_D^0, C_D^\alpha, C_D^\delta, C_D^{\alpha\delta}, C_D^{\alpha^2}, C_D^{\delta^2}, C_D^{Ma}$ are the adjusted parameters concerning the drag coefficient C_D; $C_m^0, C_m^\alpha, C_m^\delta, C_m^{\alpha\delta}, C_m^{\alpha^2}, C_m^{\delta^2}, C_m^{Ma}$ are the adjusted parameters concerning the pitch moment coefficient; $C_T^0, C_{T,\phi}^\alpha, C_{T,\phi}^{\alpha Ma}, C_{T,\phi}^{Ma}$ s, $C_T^\alpha, C_T^{\alpha Ma}, C_T^{Ma}$ are the adjusted parameters concerning the propulsive coefficient C_T; α, δ_e indicate the angle of attack and elevator deflection angle, respectively. Based on these force and moment coefficients, the lift force L, drag force D, thrust T, and pitch moment M_y can be calculated by

$$\begin{cases} L = 0.5\rho v^2 sC_L \\ D = 0.5\rho v^2 sC_D \\ T = 0.5\rho v^2 A_e C_T \\ M_y = 0.5\rho v^2 s\bar{c}C_m, \end{cases} \tag{13}$$

where $\rho, s, \bar{c}$ are, respectively, the air density, reference area, and mean aerodynamic chord; v, A_e represent the flight speed and capture area of the engine, respectively. Once these forces and moments are acquired, the dynamic model of hypersonic vehicles can be established as [29]

$$\begin{cases} \dot{v} = \frac{T\cos\alpha-D}{m} - g\sin\gamma \\ \dot{\gamma} = \frac{L+T\sin\alpha}{mv} - \frac{g\cos\gamma}{v} \\ \dot{h} = v\sin\gamma \\ \dot{\alpha} = q - \dot{\gamma} \\ \dot{q} = \frac{M_y}{I_{yy}}, \end{cases} \tag{14}$$

where γ, h, q denote, respectively, the flight path angle, flight altitude, and pitch angle rate; m, g, I_{yy} indicate the mass, acceleration of gravity, and moment of inertia, respectively. Furthermore, the nonlinear model of Eqs. (13) and (14) can be linearized for the given trim point, and the according linear model is written as

$$\dot{X} = AX + BU, \tag{15}$$

where $x^T = [v, \gamma, h, \alpha, q]$ and $u^T = [\delta_e, \phi]$. In addition, A, B are computed as [30]

$$A = \begin{bmatrix} X_v & X_\alpha + g & X_h & 0 & -g \\ \frac{Z_v}{v} + \frac{Z}{v^2} - \frac{g}{v^2} - \frac{1}{R_E+h} & \frac{Z_\alpha}{v} & \frac{Z_h}{v} + \frac{v}{(R_E+h)^2} & 1 & 0 \\ 0 & -v & 0 & 0 & v \\ \frac{M_v}{I_{yy}} & \frac{M_\alpha}{I_{yy}} & \frac{M_h}{I_{yy}} & 0 & 0 \\ 0 & 0 & 0 & 1 & 0 \end{bmatrix}, \quad (16)$$

$$B = \begin{bmatrix} D_{\delta_e} & T_\phi \\ \frac{Z_{\delta_e}}{v} & \frac{Z_\phi}{v} \\ 0 & 0 \\ M_{\delta_e} & M_\phi \\ 0 & 0 \end{bmatrix}. \quad (17)$$

Based on the obtained linear model, the transfer function γ corresponding to δ_e can yield as

$$\frac{\gamma}{\delta_e} = \frac{A_\gamma \left(z + \frac{1}{T_{\gamma 1}}\right)\left(z + \frac{1}{T_{\gamma 2}}\right)\left(z + \frac{1}{T_{\gamma 3}}\right)}{\left(s + \frac{1}{T_{sp1}}\right)\left(s + \frac{1}{T_{sp2}}\right)\left(s + \frac{1}{T_{p1}}\right)\left(s + \frac{1}{T_{p2}}\right)\left(s + \frac{1}{T_h}\right)}. \quad (18)$$

The transfer function in Eq. (18) has five poles, including the long period mode for two poles, two the short period mode for two poles, and the high mode for one pole. Also, there are three zeros, which include a pair of conjugate root and a root near zero. In particular, the specific poles and zeros can be expressed by

$$z_{\gamma 2,3} = \pm\sqrt{M_\alpha + \frac{Z_\alpha M_{\delta_e}}{Z_{\delta_e}}}, \quad (19)$$

$$s_{sp1,2} = \frac{Z_a}{2v} \pm \frac{\sqrt{Z_a^2 + 4v^2 M_a}}{2v} \approx \frac{Z_a}{2v} \pm \sqrt{M_a}. \quad (20)$$

In general, Z_{δ_e} always decreases with the increase of the angle of attack, namely $Z_\alpha < 0$. For the waverider configuration, the ratio between the elevator moment and the elevator lift $M_{\delta_e}/Z_{\delta_e}$ is close to zero, so there are unstable pole and zero in Eq. (18). Beyond this, the unstable pole and zero are interrelated with aerodynamic derivatives, thereby having a great influence on the flight performance. More importantly, the satisfactory flight qualities depend on the flight condition and states, and the overall performance will improve accordingly by optimizing the flight condition. To this end, the optimization issues on hypersonic vehicles will be considered in the following sections.

4 Optimization Design with Integrated Performances for Hypersonic Vehicles

The selection of the cruise state is the key point in the design of flight controller. The optimal cruise point is related to the performance index, which is specified by the specific flight mission. Cruise performance indexes include maximum lift-to-drag ratio in the given range, minimum fuel consumption per unit range, maximum flight distance, and maximum flight endurance. In this study, the maximum lift-to-drag ratio in cruise phase is chosen as the objective function for HSVs in combination of the improved PIO algorithm.

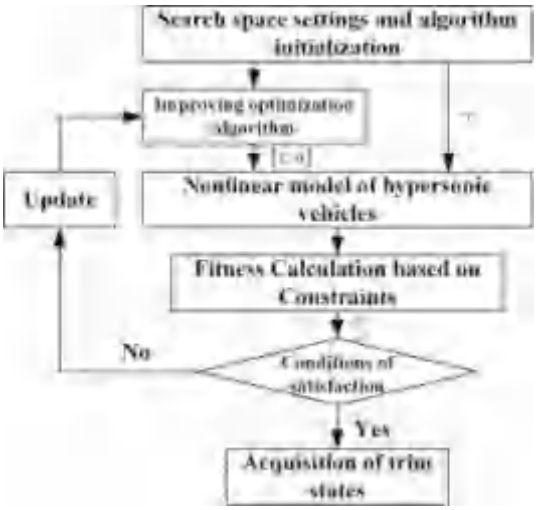

Fig. 3 The optimization course of trim states

A two-stage optimization strategy is conducted to achieve the best lift-to-drag ratio cruise state for HSVs. The first-stage optimization involves determining the equilibrium state and control values at the given flight height and velocity; the second stage aims to optimize the flight state to obtain the best cruise point.

(1) Equilibrium-state optimization using PIO

In the equilibrium state, the velocity and angular velocity are equal to zero or a given value, and the acceleration is set to zero. Based on that, the longitudinal cruise equilibrium-state optimization is changed as the straight-level flight problem, thereby satisfying the following constraints $\dot{v}, \dot{\gamma}, \dot{h}, \dot{\alpha}, \dot{q} = 0$. Furthermore, the dynamic-integral objective function in this work is employed as

$$J = \int_0^{t_f} \eta(\beta_1 |\dot{v}| + \beta_2 |\dot{\gamma}| + \beta_3 |\dot{h}| + \beta_4 |\dot{\alpha}| + \beta_5 |\dot{q}|)\mathrm{d}t, \quad (21)$$

where t_f is the terminal time; η is the dynamic weight used to weaken the unstable mode accumulated with time; and the coefficients $\beta_i, i = 1, 2 \ldots, 5$ make that each state derivative index can reach optimal values. Accordingly, the optimization course is depicted in Fig. 3.

(2) Cruise condition optimization using PIO

The optimization index in cruise phase is selected as the maximum lift-to-drag ratio, which is related to flight states and control inputs. In principle, the cruise state is expected to generate maximum lift-to-drag ratio to reduce fuel consumption and to improve flight efficiency.

The optimization constraints of the cruise condition include the dynamic equation, flight state, control saturation, and dynamic pressure limitation. With the limitations of the flight envelope, elevator deflection range, and engine throttle, the flight state and control saturation constraints are given as [29]

$$\begin{cases} h_{\text{low}} \le h \le h_{\text{up}} \\ v_{\text{low}} \le v \le v_{\text{up}}, \end{cases} \tag{22}$$

$$\begin{cases} \delta_{e_{\text{low}}} \le \delta_e \le \delta_{e_{\text{up}}} \\ \phi_{\text{low}} \le \phi \le \phi_{\text{up}}. \end{cases} \tag{23}$$

Flight stability depends on enough dynamic pressure to maintain normal flight, and the constraint of the minimum dynamic pressure is

$$P = 0.5\rho v^2 > P_{\text{low}}. \tag{24}$$

To this end, the optimization function concerning the cruise state is

$$\min J = -C_L/C_D, \tag{25}$$

where C_L and C_D are the lift and drag coefficients, respectively. Furthermore, the optimization process of the cruise condition is provided as Fig. 4.

(3) Trajectory optimization using PIO

Typically, the trajectory optimization problem of HSVs include the dynamic pressure constraints, path constraints, and terminal constraints. According to the above-mentioned dynamic model, the dynamic pressure constraints combined with Eq. (14) are written as

$$\begin{cases} \frac{dr_c}{dt} = v\cos\theta\frac{R_g}{R_g+h} \\ \frac{dm}{dt} = -\frac{T}{I_{sp}g_0}, \end{cases} \tag{26}$$

where r_c and R_g show the flight range and the earth radius respectively; I_{sp} and g_0 are the specific impulse and gravitational acceleration constants, respectively.

During flight, the atmosphere friction generates massive heat. To prevent overheating, the heating rate limitation is given as

$$\dot{Q} = C\rho^N v^K \le \dot{Q}_{\max}, \tag{27}$$

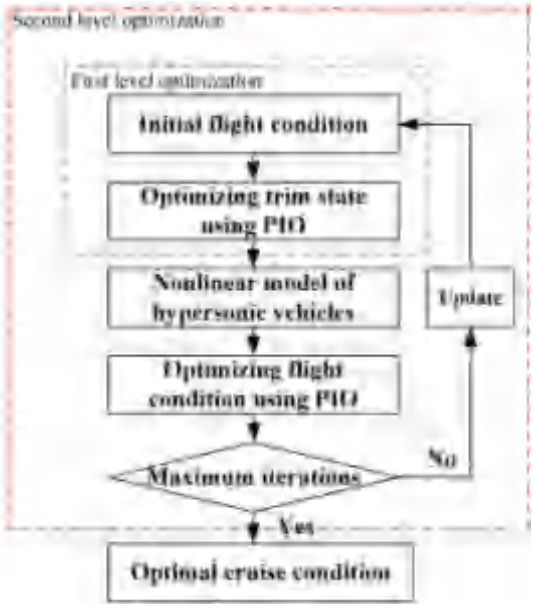

Fig. 4 Design process of optimal cruise condition

where C, N, and K represent the selected parameters for aerodynamic thermal constraints.

The aerodynamic load is a critical constraint on the normal acceleration, which is described as

$$n = \frac{\sqrt{L^2 + D^2}}{mg_0} \le n_{\max}. \tag{28}$$

The dynamic pressure must also not exceed the limit of the vehicle's mechanical protection

$$P = 0.5\rho v^2 \le P_{\max}. \tag{29}$$

The terminal constraints are associated with flight task. In this study, the terminal velocity and altitude are required for reaching the final cruise condition

$$\begin{cases} h(f) \in h_f \pm \Delta h \\ v(f) \in v_f \pm \Delta v \\ \theta(f) = \theta_f. \end{cases} \tag{30}$$

Subject to the dynamic equation of motion, the goal of the climbing trajectory optimization in this research is to find a control strategy in which the most fuel-efficient constrained climbing trajectory can be generated while satisfying all the optimal constraints. The objective function is described as

$$\min J = -m_f, \tag{31}$$

where m_f represents the terminal remaining mass of the vehicle. The aim of the optimal strategy is to minimize the fuel consumption in the climbing phase as a result that path

Table 1 The geometric parameters of hypersonic vehicles

Names	Values	Names	Values	Names	Values	Names	Values
L_{fore}	14 m	L_{mid}	5.9 m	L_{aft}	10 m	H_{c1}	1.02 m
H_{c2}	2.4 m	H_b	3 m	H_{fore}	0.9 m	H_{mid}	0.96 m
H_{aft}	0.84 m	H_e	1.2 m	H_{ni}	1.8 m	H_{no}	0.3 m
W_{fore}	3 m	W_{mid}	6 m	W_{aft}	6 m	W_{nozzle}	6 m
m	42,094 kg	I_{yy}	973,466kg m^2	a_{ref}	21 m	$\bar{c}$	1.5 m
W_{eng}	2.4 m	L_{c1}	8 m	L_{cowl}	2 m		

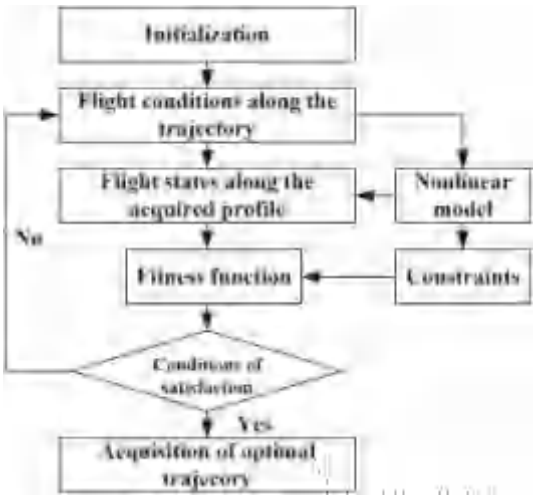

Fig. 5 The flowchart of the trajectory optimization

constraints, terminal constraints, and state constraints are satisfied with the given nonlinear model of hypersonic vehicles. The optimal problem is expressed by

$$\begin{cases} \min J = \Phi\left(\mathbf{X}\left(\mathbf{t_f}\right), t_f\right) \\ \text{s.t.} \begin{cases} \dot{\mathbf{X}}(\mathbf{t}) = F\left(\mathbf{X}\left(\mathbf{t}\right), \mathbf{U}\left(\mathbf{t}\right), t\right) \\ C\left(\mathbf{X}\left(\mathbf{t}\right), \mathbf{U}\left(\mathbf{t}\right), t\right) \le 0 \\ \varphi\left(\mathbf{X}\left(\mathbf{t_0}\right), \mathbf{X}\left(\mathbf{t_f}\right), t_0, t_f\right) = 0, \end{cases} \end{cases} \tag{32}$$

where $\varphi\left(\mathbf{X}\left(\mathbf{t_0}\right), \mathbf{X}\left(\mathbf{t_f}\right), t_0.t_f\right) = 0$ is gotten based on the boundary constraints, whereas $J = \Phi\left(x_{t_f}, t_f\right)$ is determined by the objective function. In this study, the constrained trajectory optimization problem can be transformed into unconstrained optimization problem in line with the aforementioned constraints, and the optimal trajectory can be obtained by iterating the performance index function. Correspondingly, the flow chart of the trajectory optimization design using pigeon swarm intelligent optimization algorithm is provided as Fig. 5.

After identifying the optimized trajectory, the controller needs to be designed to suppress the uncertain disturbances and to follow the expected trajectory. To this end, a trajectory tracking controller based on LQR optimal control theory is proposed for hypersonic vehicles to ensure robust stability and tracking performance. In particular, the control system

Table 2 The sampling range of hypersonic vehicles

Parameters	Minimum value	Maximum value
h	14, 000 m	32, 000 m
Ma	4	15
α	$-6°$	$8°$
δ_e	$-10°$	$10°$
ϕ	0.2	1.2

is designed as follows:

$$\mathbf{u}^*(\mathbf{t}) = -\mathbf{k_{opt}}\mathbf{x}(\mathbf{t}), \tag{33}$$

$$\mathbf{k_{opt}} = \mathbf{R}^{-1}(\mathbf{t})\mathbf{B}^{\mathbf{T}}(\mathbf{t})\mathbf{P}(\mathbf{t}), \tag{34}$$

where $\mathbf{P}(\mathbf{t})$ is solved by

$$\begin{aligned} \dot{\mathbf{P}}(\mathbf{t}) = &-\mathbf{P}(\mathbf{t})\mathbf{A}(\mathbf{t}) - \mathbf{A}^{\mathbf{T}}(\mathbf{t})\mathbf{P}(\mathbf{t}) \\ &+\mathbf{P}(\mathbf{t})\mathbf{B}(\mathbf{t})\mathbf{R}^{-1}(\mathbf{t})\mathbf{B}^{\mathbf{T}}(\mathbf{t})\mathbf{P}(\mathbf{t}) - \mathbf{Q}(\mathbf{t}), \end{aligned} \tag{35}$$

where Q and R indicate the weight matrix to make the following index optimal:

$$J = \frac{1}{2}\int_0^t \left[\mathbf{x}^{\mathbf{T}}(\mathbf{t})\mathbf{Q}(\mathbf{t})\mathbf{x}(\mathbf{t}) + \mathbf{u}^{\mathbf{T}}(\mathbf{t})\mathbf{R}(\mathbf{t})\mathbf{u}(\mathbf{t})\right]\mathrm{d}t. \tag{36}$$

In fact, the nonlinear model is first linearized on the basis of the state and control variables along the reference trajectory that is optimized using the PIO algorithm. Followed that, the controller is designed for hypersonic vehicles to realize the reference trajectory tracking. More important, the control action can relieve the uncertain effects and follow the anticipated trajectory as a result that the optimal results in Eq. (31) can be obtained and implemented for hypersonic vehicles.

5 Simulation Analysis

In parametric shape design of hypersonic vehicles, geometric parameters must be enough to ensure the fidelity of the design. On the other hand, the design parameters must not be too many to satisfy the calculation efficiency. To this end, the geometric parameters in Fig. 1 are selected as Table 1 [26].

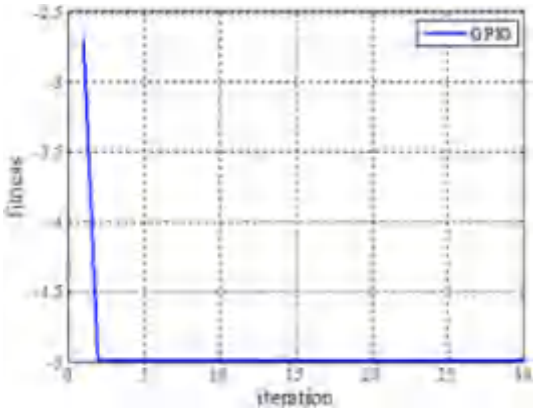

Fig. 6 The variation in fitness with iteration

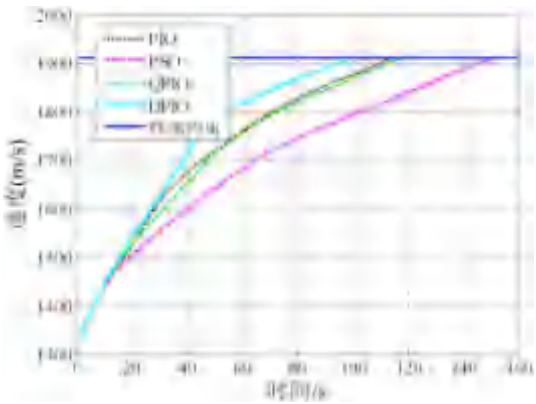

Fig. 7 The optimization results of the climbing trajectory

In addition, the aerodynamic and thrust datum of the sample points is constructed using the Latin hypercube method, and the sampling range is shown in Table 2.

The coefficients of the aerodynamic and thrust models are identified over the given range in Table 2 using the system identification method, and the specific coefficients are shown in Table 3 [26].

Based on these model parameters in Tables 1 and 3, the equilibrium values and their eigenvalues with respect to the different flight speeds and heights are listed in Table 4.

Table 4 shows that the trim fuel equivalence ratio and elevator deflection angle increase gradually with the increase of the flight altitude and Mach number. In addition, there is a pole on the right half plane, and this indicates that the model is unstable within the given flight range, such that the system design becomes a very challenging task for the waveriding configuration.

Furthermore, comparison results between intelligent optimization and algebraic calculation are provided in Table 5 to reflect the effectiveness for solving the equilibrium-state optimization problem.

Results show that the state remains constant in a short time range at the optimal solution, and the improved PIO algorithm can solve the equilibrium-state optimization problem.

Furthermore, the improved PIO algorithm is applied here to obtain the best cruise state for the maximum lift-to-drag ratio. In particular, the population size is 100 in the simulation, the dimension of optimization variables is 10, and the maximum iteration number is set to 150. Correspondingly,

Table 3 The coefficients of the aerodynamic and thrust models

	C_L^0	C_L^α	C_L^δ				
C_L	0.8203	27.5526	2.6220				
	C_D^0	C_D^α	C_D^δ	$C_D^{\alpha\delta}$	$C_D^{\alpha^2}$	$C_D^{\delta^2}$	C_D^{Ma}
C_D	0.05358	5.0155	0.3571	1.0449	0.0854	-0.0172	0.3628
	C_m^0	C_m^α	C_m^δ	$C_m^{\alpha\delta}$	$C_m^{\alpha^2}$	$C_m^{\delta^2}$	C_m^{Ma}
C_m	−0.0608	10.0624	−0.8192	1.4920	7.5885	-2.6589	0.0368
	C_T^0	$C_{T,\phi}^\alpha$	$C_{T,\phi}^{\alpha Ma}$	$C_{T,\phi}^{Ma}$	C_T^α	$C_T^{\alpha Ma}$	C_T^{Ma}
C_T	−0.8277	−16.8277	227.667	16.0146	6.6595	-81.6143	5.914

Table 4 The equilibrium values and their eigenvalues for different speeds and heights

$[Ma, h]$	$[v, \gamma, h, \alpha, q]$	$[\delta_e, \phi]$	Characteristic roots
[5, 15]	[1475, 0, 15, −0.0095, 0]	[0.065, 0.125]	$[-7.05, 6.84, 0.0019 \pm 0.0360i, -0.0022]$
[7, 18]	[1855, 0, 18, −0.0106, 0]	[0.076, 0.354]	$[-7.36, 7.21, 0.0145 \pm 0.0675i, -0.0052]$
[9, 21]	[2664, 0, 21, −0.0151, 0]	[0.088, 0.475]	$[-8.65, 8.53, 0.0287 \pm 0.0907i, -0.0126]$
[11, 24]	[3267, 0, 24, −0.0149, 0]	[0.095, 0.545]	$[-8.69, 8.61, 0.0308 \pm 0.0996i, -0.0130]$

Table 5 Comparison results between intelligent optimization and algebraic calculation

Methods	Trim flight states	Trim control inputs
Improved PIO	$[v, \gamma, h, \alpha, q] = [2664, 0, 21{,}000, -0.0149, 0]$	$[\delta_e, \phi] = [0.089, 0.473]$
Algebraic calculation	$[v, \gamma, h, \alpha, q] = [2664, 0, 21{,}000, -0.0149, 0]$	$[\delta_e, \phi] = [0.089, 0.473]$

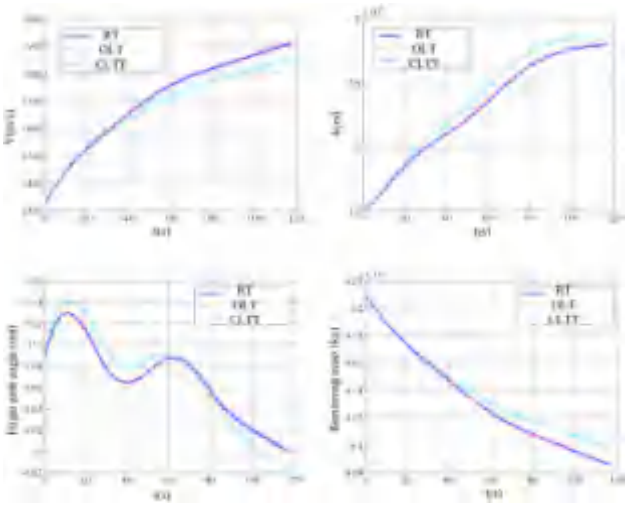

Fig. 8 Tracking responses of the climbing trajectory

the optimal results and the variation in fitness with iteration are listed in Fig. 6.

With the implementation of the improved PIO algorithm, the best cruise state for the HSV is achieved with $[v, h] = 1901m/s, 28{,}000m$. At this state, the vehicle can obtain maximum lift-to-drag ratio of 5, and this fuel-efficient state is set to be the terminal state for the climbing trajectory design. To this end, the following work implements the Gaussian mutation-based PIO algorithm to the climbing trajectory optimization problem for HSVs to verify its feasibility end effectiveness. Also, the initial flight condition and constraints are listed in Table 6.

For persuasiveness and reliability, four algorithms, including the PIO algorithm, the improved PIO algorithm using the quantum evolutionary method (QPIO), DPIO, and particle swarm optimization algorithm (PSO), are used for the comparative study, and four independent simulation works are conducted for the trajectory optimization. Accordingly, these optimal results using four algorithms are listed in Fig. 7.

Figure 7 shows that the better solution for HSVs' trajectory optimization and HSVs' flight controller design is the improved PIO algorithm compared with the classical PIO as well as PSO algorithm. Compared with these of PSO, the best fitness is lower, and response time to the given command is shorter using the improved PIO algorithm. Furthermore, these results show that the improved PIO algorithm are suitable for trajectory design and satisfy all the expected constraints.

Furthermore, the velocity command regarding the trim value is set as 50 m/s, and the response curves concerning the open-loop and closed-loop conditions are given as Fig. 8 using the LQR controller. Corresponding, the change curves in relation to the reference trajectory (RT), open-loop trajectory (OLT), and closed loop LQR trajectory (CLLT) are given in Fig. 8.

The results of Fig. 8 demonstrate that the LQR trajectory tracking controller can correct the trajectory deviation caused by the initial state error between RT and OLT, and realize the effective tracking of the flight trajectory for hypersonic vehicles.

6 Conclusions

In this work, the constrained climbing trajectory optimization problem for HSVs is established. To this end, the improved PIO algorithm is designed based on the idea of genetic algorithm, and the Gaussian mutation operation is used to ensure the diversity of the population instead of avoid falling into local optimization. Furthermore, the improved PIO algorithm is applied to solve the optimization problem, and comparative numerical simulation shows that the improved PIO algorithm is superior to the original optimization algorithm and is therefore a highly valuable engineering method for hypersonic vehicles.

Table 6 The initial flight condition and constraints

Parameters	Values
Initial flight condition	$[v, h, r, \gamma, m] = [1327$ m/s, 15,000 m, 0, 0.087 rad, 42,094 kg$]$
Terminal constraints	$v_f = 1910$ m/s, $h_f = 28{,}000$ m, $\gamma_f = 0$
Path constraints	$[\dot{Q}_{\max}, q_{\max}, n_{\max}] = [600$ kW/m^2, 50–300 kPa, 7$]$
Control constraints	$-6° \le \alpha \le 8°, -10° \le \delta_e \le 10°$

Acknowledgements This work is supported by Fundamental Research Funds for the Central Universities under Grant No. NS2021061.

Declarations

Conflict of Interest On behalf of all authors, the corresponding author states that there is no conflict of interest.

References

1. Chen K, Pei SS, Shen FQ et al (2021) Tightly coupled integrated navigation algorithm for hypersonic boost-glide vehicles in the LCEF frame. Aerospace 8:124
2. Chen B, Chen J, Liu Y et al (2020) Guardian maps based robust stability analysis with applications in flight control of hypersonic vehicles. Aerosp Sci Technol 106:106208
3. Bowcutt KG (2015) Multidisciplinary optimization of airbreathing hypersonic vehicles. J Propuls Power 17:1184–1190
4. Whitmer C, Kelkar A, Vogel J, et al. (2010) Control centric parametric trade studies for scramjet-powered hypersonic vehicles. In: AIAA guidance, navigation, and control conference, pp 1–29
5. Yokoyama N, Suzuki S, Tsuchiya T et al (2007) Multidisciplinary design optimization of space plane considering rigid body characteristics. J Propuls Power 44:121–131
6. Zhu JW, Liu LH, Tang GJ, Bao WM (2015) Highly constrained optimal gliding guidance. Proc Inst Mech Eng Part G J Aerosp Eng 229:2321–2335
7. Brown NF, Olds JR (2012) Evaluation of multidisciplinary optimization techniques applied to a reusable launch vehicle. J Spacecr Rocket 43:1289–1300
8. Lyu Y, Tang H, Chen M (2016) A study on combined variable geometries regulation of adaptive cycle engine during throttling. Appl Sci 6:374
9. Wang ZG, Huang W, Yan L (2014) Multidisciplinary design optimization approach and its application to aerospace engineering. Chin Sci Bull 59:5338–5353
10. Ghoman SS, Kapania RK, Chen PC et al (2012) Multifidelity, multistrategy, and multidisciplinary design optimization environment. J Aircraf 49:1255–1270
11. Ahuja V, Hartfield RJ (2009) Optimization of air-breathing hypersonic aircraft design for maximum cruise speeds using genetic algorithms. In: 16th AIAA/DLR/DGLR international space planes and hypersonic systems and technologies conference. pp 1–18
12. Patnaik SN, Coroneos RM, Hopkins DA et al (2002) Lessons learned during solutions of multidisciplinary design optimization problems. J Aircraftr 39:386–393
13. Fan Y, Zhu W, Bai GA (2016) A cost-effective tracking algorithm for hypersonic glide vehicle maneuver based on modified aerodynamic model. Appl Sci 46:312
14. Zhao J, Zhou R, Jin XL (2014) Progress in reentry trajectory planning for hypersonic vehicle. J Syst Eng Electron 25:627–639
15. Rizvi STU, He LS, Xu DJ (2015) Optimal trajectory analysis of hypersonic boost-glide waverider with heat load constraint. Aircr Eng Aerosp Technol 87:67-78
16. Zhang D, Liu L, Wang YJ (2015) On-line ascent phase trajectory optimal guidance algorithm based on pseudo-spectral method and sensitivity updates. J Navig 68:1056–1074
17. Liu X, Shen Z, Lu P (2016) Entry trajectory optimization by second-order cone programming. J Guid Control Dyn 39:227–241
18. Dutta P, Bhattacharya R (2010) Nonlinear estimation of hypersonic state trajectories in Bayesian framework with polynomial chaos. J Guid Control Dyn 33:1765–1778
19. Antonakis A, Nikolaidis T, Pilidis P (2017) Multi-objective climb path optimization for aircraft/engine integration using particle swarm optimization. Appl Sci 7:22
20. Duan HB, Li ST (2015) Artificial bee colony-based direct collocation for reentry trajectory optimization of hypersonic vehicle. IEEE Trans Aerosp Electron Syst 51:615–626
21. Duan H, Qiao P (2014) Pigeon-inspired optimization: a new swarm intelligence optimizer for air robot path planning. Int J Intell Comput Cybern 7:24–37
22. Duan H, Wang X (2015) Echo state networks with orthogonal pigeon-inspired optimization for image restoration. IEEE Trans Neural Netw Learn Syst 27:365–369
23. Qiu HX, Duan HB (2015) Multi-objective pigeon-inspired optimization for brushless direct current motor parameter design. Sci China Technol Sci 58:1915–1923
24. Lei XJ, Ding YL, Wu FX (2016) Detecting protein complexes from DPINs by density based clustering with Pigeon-inspired optimization algorithm. Sci China Inf Sci 59:070103
25. Jiao B, Lian Z, Gu XA (2008) Dynamic inertia weight particle swarm optimization algorithm. Chaos Solitons Fract 37:265–278
26. Chen B, Liu Y, Shen H et al (2016) Surrogate modeling of a 3D scramjet-powered hypersonic vehicle based on screening method IFFD. Proc Inst Mech Eng Part G J Aerosp Eng 231:698–705
27. Dalle DJ, Torrez SM, Driscoll JF et al (2014) Minimum-fuel ascent of a hypersonic vehicle using surrogate optimization. J Aircr 51:312–325
28. Parker JT, Serrani A, Yurkovich S et al (2007) Control-oriented modeling of an air-breathing hypersonic vehicle. J Guid Control Dyn 30:856–869
29. Liu ZY, Li ZY (2021) L1 adaptive loss fault tolerance control of unmanned hypersonic aircraft with elasticity. Aerospace 8:176
30. Colgren R, Keshmiri S, Mirmirani M (2009) Nonlinear ten-degree-of-freedom dynamics model of a generic hypersonic vehicle. J Aircr 46:800–813